Chapter 5

Impact of stellar micro-variability on transit detection from space

5.1 Introduction

This chapter summarises a number of simulations which were performed with the tools developed in the previous three Chapters. These simulations were run at different times during the period 2001–2004, so that both filtering and transit detection tools, and the mission parameters which enter into the simulations, change from section to section. The purpose of the simulations also varied, and this affects the choice of method in terms of parameter space coverage and level of detail and accuracy sought.

Section 5.2 describes simulations carried out in early 2003, in preparation for the 2nd *Eddington* workshop, which took place in April 2003. One of the main issues to be discussed at this workshop was the choice of target field for *Eddington*, and these simulations were aimed at identifying which types of planet-host stars would be favourable targets, and which would be too variable for transits of habitable planets to be detectable. At that time, the development of both variability filters and transit search algorithms was less advanced, in particular in terms of computational efficiency, so that full Monte Carlo simulations over a large grid of configurations were not feasible. A "quick look" approach was therefore adopted, in which the results from single realisations of each studied case are taken as indicative of the trends one is trying to identify, but no attempt is made to derive quantitative error rates.

Section 5.3 describes simulations carried out in late 2003 with the aim of assessing the performance of the box-shaped transit finder in combination with the non-linear filter, in the presence of stellar variability. Increased efficiency meant that Monte Carlo simulations were now feasible, but there was no need to repeat the

parameter space exploration of Section 5.2. Instead, a few targeted configurations, known to be close to the detectability limit, were used. A small number of similar simulations for the COROT case were also computed for the 5th COROT Week, which took place in December 2003, and are included in this section.

Photon noise was included (using a Gaussian approximation, which is appropriate in all the cases considered here) as expected for the missions concerned given their baseline design at the time of the simulations, and stellar micro-variability was included using the simulator developed in Chapter 3. No instrumental noise was considered. Transit signals were generated using the Universal Transit Modeller (UTM) of Deeg et al. (2001).

5.2 Simulations to identify the best target stars for *Eddington*

These simulations include:

- photon noise as expected for the *Eddington* baseline design as it stood in early 2003[1]. The design has not changed since, but it differs from that used in older, photon noise simulations presented in Chapter 2;
- stellar variability light curves generated using the simulator presented in Chapter 3, but with an older version of the activity-variability relation (dashed line on Figure 3.6);
- transit light curves generated using UTM (Deeg et al. 2001).

For a given star-planet configuration, a single realisation of the light curve was generated. It was then filtered using the optimal filter of Carpano et al. (2003), which is also discussed in Section 4.2, and an early version of the box-shaped transit finder discussed in Chapter 2 was applied. This version was identical in its results, but computationally less optimised (the improvements to the implementation described in Section 2.2.3 had not yet been made). The planet was deemed detectable in that configuration if the peak in the detection statistic corresponded to the period and epoch of the input transit, and undetectable if not. In some cases, harmonics of the true period produced higher peaks than the period itself. These cases were also considered detectable.

[1]The payload was constituted by a set of 4 identical wide field telescopes, with identical white light CCD cameras at the focal plane. In practice, this is equivalent to a single monolithic telescope with the same collecting area as the sum of the collecting areas of the 4 individual telescopes. The total collecting area of the baseline payload design was 0.764 m^2, and the field of view has a diameter of 6.7°. The CCD chips were from E2V , with the standard "broad band" response.

5.2.1 Which are the best target stars for *Eddington*?

The aim here is to identify, for example, those stars which are likely to be so variable that the detection of terrestrial planets orbiting them by *Eddington* (and by extension *Kepler*) will be seriously hindered, or on the contrary where the transits are easily recovered even in the presence of variability. This will be used to optimise both the choice of target field and the observing strategy, so that the range of apparent magnitudes containing most of the best target stars is well covered.

Light curves were therefore generated for a grid of star ages (0.625, 1.0, 2.0, 3.0 & 4.5 Gyr) and types (F5, F8, G0, G2, G5, G8, K0, K2 & K5). Planetary transits were added to the light curves for 1 & 3 $R_\oplus$ and 1 $R_{\rm Jup}$ planets with periods of 30 days, 6 months, 1 year and 3 years, resulting in 37, 7, 3 and 1 transit(s) respectively. The light curves last 3 years and have a sampling of 1 hr. Two apparent magnitudes, V = 13 and V = 15, were used.

Note that the expected sampling rate is in fact closer to 10 min than 1 hr. However, this set of simulations was designed to rapidly explore the stellar parameter space to identify regions of interest. For this purpose, the light curves were generated using a longer integration time, thereby keeping them to a manageable size and maximising the contribution of stellar noise relative to photon noise on a given data point – the impact of photon noise having already been investigated previously. Later simulations, concentrating on the habitable zones of the more promising target stars, were made with 10 min sampling. The results are shown in Figure 5.1, using the notation described in Figure 5.2.

The main conclusions to be drawn from these results are:

- The detection of transits by planets with $R_{\rm pl} \leq 3\,R_\oplus$ around stars younger than 2.0 Gyr or earlier than G0 is significantly impaired, even for very high signal-to-noise ratio, and they are not good targets for the exo-planet search of *Eddington* or for *Kepler*.

- The small radius (hence increased transit depth) of K stars outweighs their relatively high variability levels, making them the best targets aside from effects not considered here, such as magnitude distribution and crowding. These will need to be assessed carefully. Whether this trend continues for M stars – recalling that they were not included in the simulations because of the significant number of fast M rotators present at Hyades age – is an open question (see Deeg 2004). Another complicating factor for these late-type stars is the need to include the effects of micro- and nano-flaring, an issue under investigation.

- Earth-sized planets are not detected correctly around G stars with 3 transits only. This is only an indicative result, but it demonstrates the need to increase

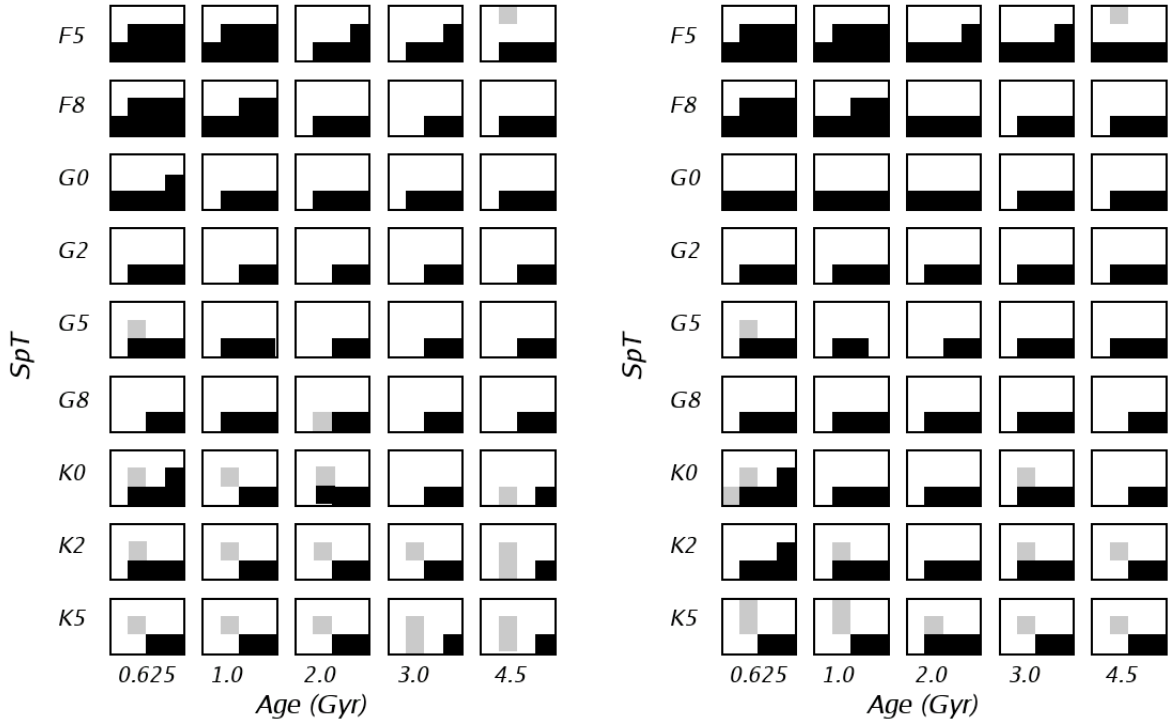

Figure 5.1: Results of the simulations with 1 hour sampling for V =13 (left) and V =15 (right). The notation used is detailed in Figure5.2.

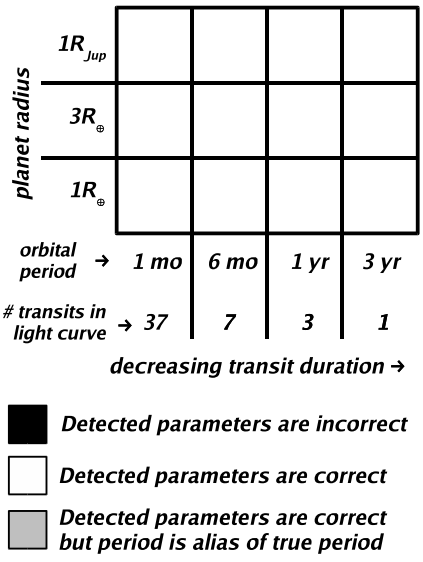

Figure 5.2: Notation used in Figure 5.1.

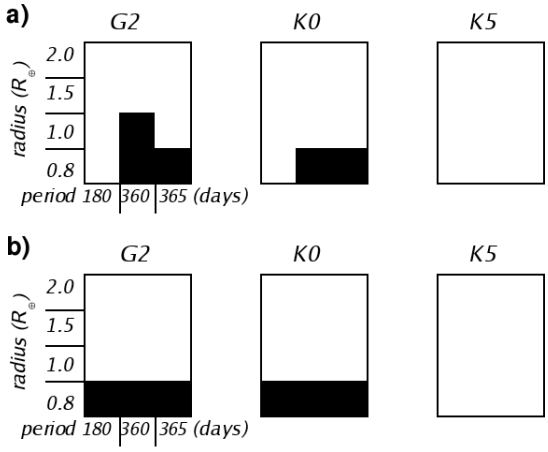

Figure 5.3: Results of the simulations with 10 min sampling for V =12 (a) and V =13 (b).

the transit energy or signal-to-noise ratio (our statistic S, cf. Section 2.2) for such systems, i.e. the square root of the number of in-transit points times the ratio of transit depth to per noise level per data point. As photon noise is not the limiting noise source at $V = 13$, increasing the collecting area would not significantly lower the noise level. Instead, one needs to increase the number of in-transit points, while keeping the noise level per data point constant. This can be achieved through longer light curve duration. Finer time sampling would increase the number of in-transit points, but also the photon noise per data point. It is thus expected to improve the results only for the bright, stellar noise dominated stars. The magnitude limit between the stellar noise and photon noise dominated regimes depends on the integration time, so that the optimum sampling rate is likely to be magnitude dependent.

- At $V = 15$ and with 1 hr sampling, photon noise has become the dominant factor for most stars.

The third point in the list above could have important consequences for the target field/star selection for *Kepler*. The current target field is centred on a galactic latitude of $\simeq 5°$ in the region of Cygnus, and was chosen to maximise the number of stars in the field while being sufficiently far from the plane of the ecliptic to allow continuous monitoring (Borucki et al. 1997). Due to telemetry constraints, which limit the number of observed stars to $\simeq$ 100 000, and to crowding, which can have a very large impact in such high density regions, only stars with $V \leq 14$ are likely to be monitored in this field. However, with its larger collecting area (corresponding to a single aperture of 0.95 m), Kepler's light curves will be star noise rather than photon noise dominated down to fainter magnitudes than in the case of *Eddington*. Given that, out of the spectral types tested here, K stars gave the best results, and that these stars tend to be fainter than earlier types, it may be desirable to choose a field at higher galactic latitude, combined with a deeper magnitude limit. It would likely be difficult to extend the magnitude limit while keeping the same target field due to increased crowding.

The final choice of target fields for both *Eddington* and *Kepler* will depend on many factors besides micro-variability and the change of stellar radii with spectral type, which are the only two effects taken into account in the present simulations. Other constraints are imposed by a number of factors. We have already discussed the impact of limited telemetry budgets, as well as that of the different apparent magnitude distributions of different stellar types, and the problems due to crowding in high density regions. Constraints arise from the luminosity class (i.e. radius) distribution of the stars in the field of view as well as from their spectral types (i.e. mass). Only fields with a large enough population of late-type (mid-F onwards) of dwarfs

are interesting for planet searches. Members of the COROT team, who have used spectrophotometry to determine the spectral type and luminosity class of fields in the potential COROT field, based on *B*, *V*, *R*, *I*, *J*, *H* & *K* information, have found that patchy reddening hampers the classification. Some candidate COROT fields in which the reddening was too spatially variable were excluded on that basis. Another important factor is the availability of ground-based facilities accessible to the scientific community involved with each mission, for further preparatory and follow-up observations. As the planet-finding target field will be close to one of the ecliptic poles, it will have a high declination and thus will be efficiently observable from either the southern or the northern hemisphere, but not both.

5.2.2 Minimum detectable transit in the presence of variability

Another question of interest is whether *Eddington* will really probe the habitable zone of the stars it targets, if micro-variability is taken into account. For this purpose, we have simulated light curves with increased sampling (10 min) for three 4.5 Gyr old stars (types G2, K0 & K5) orbited by planets with radii of 0.8, 1.0, 1.5 & 2.0 $R_\oplus$, with periods of 180, 360 & 365 days (corresponding to 7, 4 and 3 transits in the light curves respectively). The last two have very similar periods (i.e. virtually identical transit shapes and durations) but the extra transit in the 360 day case is due to the fact that the first transit occurs soon after the start of the observations. This is intended to test the effect of adding an extra year to the planet-search phase, in order to detect more transits. In white Gaussian noise, the dependence of performance on stellar and planet radius and apparent magnitude could be predicted analytically form the properties of the detection statistic employed by the transit search algorithm. However, in the presence of stellar variability, simulations are needed: one cannot assume that the noise is white and Gaussian even after filtering, particularly in the case of the more active stars.

The boundary between the stellar noise dominated and photon noise dominated regime, situated between $V = 13$ and $V = 15$ for 1 hour integration, will be approximately 1 mag brighter for 10 min integrations. In order to ensure that this second set of simulations still covered, at least in part, the stellar noise dominated regime, two values were used for the apparent magnitude of the stars: $V = 12$ and $V = 13$.

The results are shown in Figure 5.3. Generally speaking, they follow the expected trends. While the 0.8 $R_\oplus$ planet is detected provided enough transits are present at $V = 12$, it is not detected around all but the smallest star at $V = 13$, as a result of the increased level of photon noise. The Earth-sized planet is only marginally detectable with 3 or 4 transits around a G2 star, even at $V = 12$. The fact that it is detected with 4 transits but not with 3 at $V = 12$, and is detected in both cases at

V = 13, highlights the need for full Monte Carlo simulations to obtain more reliable detectability estimates. It should serve as a reminder that the present work only aims to provide a global picture of the trends with star, planet and observational parameters, rather than quantitative results. Closer inspection of the light curve containing 4 Earth-sized transits around a G2 star at V = 12 showed that two of them were superposed on parts of the light curve where the noise was consistently positive, which impeded the detection. The rate of such coincidences can only be estimated from multiple realisations of the same system. To summarise, in the stellar noise dominated regime, the minimum reliably detectable radii for G2, K0 and K5 stars are roughly 1.5, 1.0 and 0.8 $R_\oplus$ respectively with 3 or 4 transits, and 0.8 $R_\oplus$ in all cases with 7 transits.

By comparison, 'habitable' planets are usually required to have radii in the range $0.8\,R_\oplus \leq R_{\rm pl} \leq 2.2\,R_\oplus$. They are also required to lie in the habitable zone, given the following orbital distance ranges for 4.5 Gyr old stars: 0.5 to 1 AU (0.8 $M_\odot$, K2 star) and 0.9 to 1.3 AU (1.0 $M_\odot$, G2 star). Simplified calculations give the orbital period corresponding to the centre of the habitable zone, for the mass ranges of interest, as 1.2, 0.6 and 0.3 years for G2, K0 and K5 stars respectively, (see Section 1.2.3 for the rationale behind these limits).

The effect of the increased sampling rate is immediately visible. While a 'true Earth analogue' (Earth-sized planet orbiting a G2 star with a period of 1 year) may not be detected reliably, a good part of the habitable zone of the G2 star and all of that of the K0 and K5 stars are covered. This suggests that the primary goal of discovering and characterising extra-solar planets in the habitable zone will be achievable around intermediate age and old late-G and K stars with the current design. To push back these limits, modifications to the baseline design – such as the possible inclusion of colour information – have now been made. The fact that the detectability of both 1.0 and 0.8 $R_\oplus$ planets increases significantly with increased number of transits, suggests that it may be desirable to increase the duration of the planet search stage, or to return to the planet search field for confirmation after a break (during which the asteroseismology programme, the other primary goal of *Eddington*, would be carried out).

5.2.3 Relevance to *Kepler*

As discussed in Sections 1.2.3.3 and 1.2.3.4, the photometric performances and time-sampling characteristics of *Eddington* and *Kepler* are very similar. The results of the present section can therefore be considered to apply to *Kepler* as well as *Eddington*. The epoch of 360 d period case in Section 5.2.2 was chosen so as to include 4 transits in the light curves, so that it corresponds roughly to a 1 yr period planet observed with *Kepler* (pointing duration 4 yr) while the 365 d period case corresponds to the

same system observed with *Eddington*.

5.3 Performance of the non-linear filter plus box shaped transit finder

The simulations presented in this Section were carried out using the micro-variability simulator, non-linear filter and box-shaped transit finder exactly as described in Chapters 3, 4 and 2 respectively.

5.3.1 Preliminary tests

To identify the zone of parameter space of interest, that is the limiting zone between detectable and undetectable transits, single realisations of individual star-planet configurations were tested one by one before embarking on more detailed Monte Carlo simulations.

The box-shaped transit search finder was first applied to the filtered light curve shown in Figure 4.11. The results are shown in Figure 5.4. The detection is unambiguous, and remains so for a 1.5 $R_\oplus$ planet with otherwise identical parameters, though the detection is not successful for a 1 $R_\oplus$ planet with only 3 transits (the star is a 4.5 Gyr old G2 dwarf in all cases). In the latter case, the 3 combined transits would have a total *SNR* of ~ 10 in white noise only, which should be detectable, but the combined *SNR* is only ~ 6 in the filtered light curves, which places it at the detectability limit. This is due to a combination of two effects. First, the filter does not completely remove the stellar variability (illustrated by a small departure from a Gaussian in the post-filtering noise distribution). Second, to mimic a realistic situation where the exact transit duration is not known before filtering, a guess duration of 50 data points, or $\sim$ 8.3 hours, was used to filter the light curve, rather than the actual duration of $\sim$ 13 hours. As a result some of the transit signal is filtered out, reducing the central transit depth by about one fifth. In a realistic situation, one would need to make a trade-off between computing time and sensitivity to choose the appropriate trial duration sampling.

5.3.2 Monte Carlo simulations for *Eddington*

The method employed was identical to that described in Section 2.1.3.1. The detection statistic (in this case the signal-to-noise ratio of the best candidate transit) is computed for N light curves with transits. All light curves have the same parameters, but different realisations of the noise and different epochs randomly drawn from a

Table 5.1: Light curve characteristics for each panel of Figure 5.5.

Panel	a)	b)	c)	d)	e)
Photon noise	√	√	√	√	√
Stellar variability	×	√	√	√	√
Age (Gyr)	4.5	4.5	4.5	4.5	4.5
Spectral type	G2V	G2V	G2V	G2V	K5V
$R_{\rm pl}$ ($R_\oplus$)	1.0	1.0	1.5	1.0	1.0
Period (yr)	1.0	1.0	1.0	0.5	1.0

uniform distribution (the epoch should not affect the detection process). The process is repeated for N transit-less light curves, which have noise characteristics identical to those of the light curves with transits. The chosen value of 100 for N is a compromise between accuracy and time constraints, and suffices to give a reasonable estimate of the performance of the method.

As the aim was to test the combined filtering and detection process, the light curves were subjected to the iterative nonlinear filter, before being forwarded to the transit detection algorithm. To avoid prohibitively time-consuming simulations, and thus to allow several star-planet configurations to be tested, a single transit duration value was used (corresponding roughly to the FWHM of the input transits). A detection threshold in terms of multi-transit *SNR* was automatically chosen to minimise the total number of false alarms and missed detection for each star-planet configuration.

Photon-noise only case As a benchmark against which to compare the performance in the presence of stellar variability, a photon-noise only case was tested first. Previous Monte Carlo simulations with white noise only involving this algorithm (see Section 2.2.4) were based on an older version of the *Eddington* design and did not include the non-linear filter.

The chosen configuration was a 1.0 $R_\oplus$ planet orbiting a V = 13 G2V star with a period of 1 year, which as we have seen in Section 5.3.1 is at the detection limit when stellar noise is added. After a set of simulations was run for such a configuration, the maximum detection statistic from the noise only light curves was *SNR* = 5.79, while the minimum value from the light curves with transits was *SNR* = 7.41 (see Figure 5.5a). Any threshold in between would therefore allow the detection of all the transits where present, with no false alarms. As expected, the *SNR* limit of 6, established in Chapter 2, falls within the range of suitable thresholds.

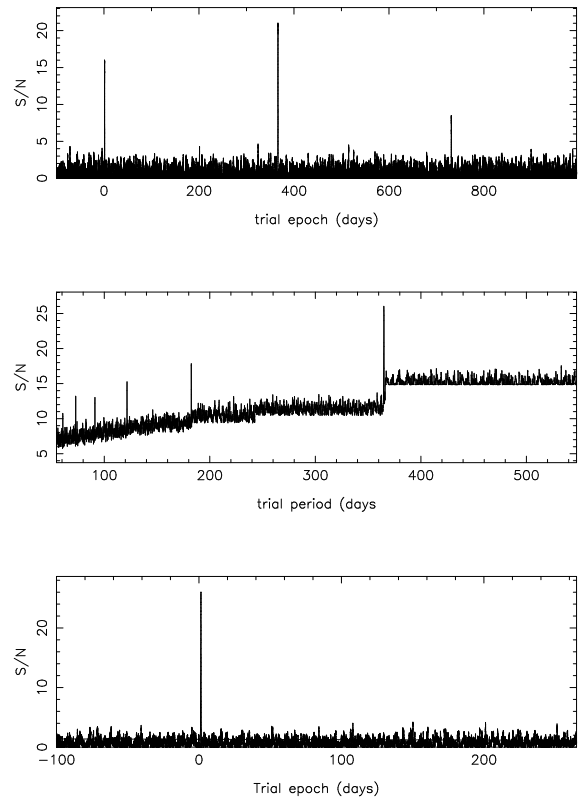

Figure 5.4: Output of the box-shaped transit finder after non-linear filtering. Top: single transit SNR as a function of trial epoch. The signature of all three transits (e = 1.5, 366.5 & 731.5 days) is clearly visible. Middle: multiple transit detection statistic as a function of trial period. Bottom: idem, as a function of epoch at the optimal period of 365.0 days. The detected epoch (1.5 day) is correct. The x-axis for the top and bottom panels were shifted by 100 days for clarity.

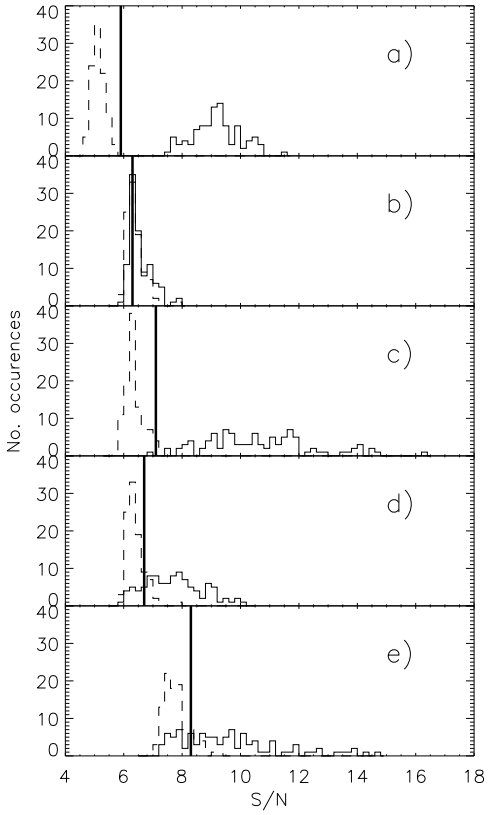

Figure 5.5: Results of the performance evaluation for 5 star-planet configurations, as detailed in Table 5.1. Solid histograms: distributions of the maximum multi-transit SNR computed by the transit detection algorithm after non-linear filtering for 100 light curves containing transits. Dashed histograms: idem for 100 light curves containing stellar variability and photon noise only. Thick vertical lines: optimal detection threshold.

Photon noise and stellar variability

• 1.0 $R_\oplus$ **planet orbiting a G2V star**
This configuration is identical to that explored in the photon noise only case, but with stellar variability added. It is also similar to the case illustrated in Figures 4.1 to 5.4, but with a smaller planet. The results are shown in Figure 5.5b. The distributions of the detection statistics from the light curves with and without transits overlap almost entirely, i.e. the performance is poor. The threshold that minimises the sum of false alarms and missed detection leads to 56 of the first and 26 of the second.

Assuming that the sampling rate, light curve duration, and stellar apparent magnitude are fixed, there are three factors which should lead to better performance: a larger planet, a shorter orbital period (i.e. more transits) or a smaller star. Each of these options in turn is investigated below.

• 1.5 $R_\oplus$ **planet orbiting a G2V star**
The histograms are relatively well separated (see Figure 5.5c), with only a small overlap, so that the optimal threshold of SNR = 7.85 leads to one missed detection and no false alarms.

It is interesting to note the similarity between the results of this simulation and the requirements used for the design of the *Kepler* mission, which was to detect planets given a signal-to-noise ratio totalling at least 8 for at least three transits[2].

• 1.0 $R_\oplus$ **planet orbiting a G2V star with 6 transits**
The aim of this set of simulations was to investigate the effect of increasing the number of transits in the light curve by a factor of two by reducing the orbital period to 182 days. This is equivalent to increasing the overall duration of the observations. As expected, this leads to higher SNR values and hence better performance, with only 13 false alarms and 16 missed detections (see Figure 5.5d).

• 1.0 $R_\oplus$ **planet orbiting a K5V star**
A K5 star is smaller than a G2 star, leading to deeper transits, but also more active, leading to more stellar variability. Parallel studies (see Section 5.2.1) suggest that the former effect prevails over the latter, and that K or even M type stars might make better targets for space missions seeking to detect habitable planets than G stars, but these are based only on results from a few individual light curves, rather than Monte Carlo simulations. We saw in the previous chapter (Section 2.2.4) that such a configuration, in the presence of photon noise only could be detected down to V = 14.5 with the older (single telescope) *Eddington* design. Can it be detected at V = 13 with stellar variability added, using the (improved) photometric performance of the new, multiple telescope design?

[2] See `www.kepler.arc.nasa.gov/sizes.html`.

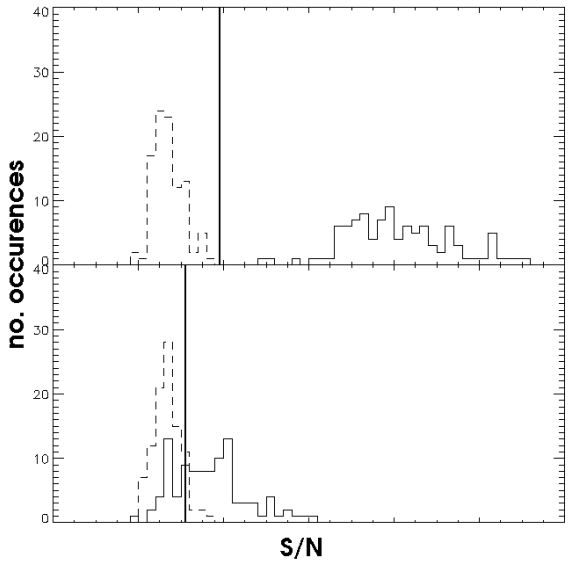

Figure 5.6: Results of the simulations for the COROT case. Top: 2.0 $R_\oplus$ planet, bottom: 1.5 $R_\oplus$ planet. The star is a 4.5 Gyr old G2V star with V =14 and the planet's orbital period is 30 days. The light curves last 150 days with 16 min sampling. Solid histograms: distributions of the maximum multi-transit SNR computed by the transit detection algorithm after non-linear filtering for 100 light curves containing transits. Dashed histograms: idem for 100 light curves containing stellar variability and photon noise only. Vertical lines: optimal detection threshold.

The present tests confirm that K-stars make good targets: the separation between the with- and without transit distributions is wider (see Figure 5.5e) than in the previous case, though the best-threshold false alarm and missed detection rates remain high at 13 and 25 % respectively.

Note the higher *SNR* values for the transit-less light curves compared to the G2 case, which suggests the presence of more residual stellar variability after filtering, as would be expected.

5.3.3 COROT simulations

Two star-planet configurations were investigated in a similar manner for the case of COROT. COROT's exo-planet program is designed to detect relatively close-in (periods of days to a month or so) terrestrial planets around main-sequence stars with magnitudes in the range $12 \leq V \leq 15$. A solar-age G2V star with $V = 14$ was therefore used here, with a 2 $R_\oplus$ or 1.5 $R_\oplus$ planet in a 30 day orbit, leading to 5 transits lasting $\sim$ 5 hours each. The first configuration is easily detected, as indicated by the top panel of Figure 5.6, but the detection is unreliable for the second.

These results are in approximate agreement with the design requirements of COROT, namely to detect 'big hot Earths', i.e. planets with radii above 2.2 $R_\oplus$ in orbits lasting a month or less. Earth-sized planets might be detectable around smaller, brighter stars given even shorter orbital period (of order 10 days). No further simulations were carried out here, because the case of COROT is investigated in a much more detailed manner in Chapter 6.

5.4 Discussion

Light curves were simulated for single realisations of a large grid of star-planet configurations, including stellar micro-variability and photon noise as expected for *Eddington*. After optimal (or matched) filtering, the results of transit searches on these light curves suggest that stellar micro-variability, combined with the change in stellar radius with spectral type, will make the detection of terrestrial planets around F-type stars very difficult. On the other hand, K-stars appear to be promising candidates despite their high variability level, due to their small radius.

At V = 12 and with 10 min sampling, the smallest detectable planetary radii for 4.5 Gyr old G2, K0 and K5 stars, given a total of 3 or 4 transits in the light curves, were found to be 1.5, 1.0 and 0.8 $R_\oplus$ respectively. This result was obtained in stellar noise rather than photon noise dominated light curves, and therefore also applies to lower apparent magnitudes or larger collecting areas. The magnitude limit beyond which photon noise would start to dominate, thereby increasing the minimum detectable radii for a given star and observing configuration, depends on the collecting area and sampling time, but the effects of increased photon noise are detected at V = 13 for 10 min sampling time and *Eddington*'s collecting area.

Full Monte Carlo simulations were run for a smaller number of configurations with the aim of assessing the performance of the box-shaped transit finder of Chapter 2 combined with the non-linear filter. From these it can be concluded that, if all or most of the stellar noise can be filtered out (so that the distribution of the detection statistic maxima in the noise-only light curves resembles that obtained for the photon-noise only case), any transit signal leading to a combined $SNR \geq 6$ can be detected. If residual stellar signal is present, the minimum detectable SNR is proportionally increased.

Most – though not all – of the stellar signal can be removed for G2 solar age stars, but a significant fraction of the stellar signal escapes the filtering for a solar age K5 star. In the latter case the detection performance could be improved by selecting transit candidates not only according to their combined SNR, but according to the ratio of combined to single-transit SNR, as the spurious SNR peaks due to stellar variability mostly arise from single events. The filter also does remove a small portion of the transit signal. These Monte Carlo simulations confirm that a 1.0 $R_\oplus$ planet orbiting a solar age, V = 13 G2 star will be difficult to detect for *Eddington*. Improvements on this result can be sought along several directions: improved filtering, better candidate selection, and increases in the telescope collecting area (to reduce photon noise) and/or in the duration of the mission (cf. the 4 year mission lifetime for *Kepler*).

Full Monte Carlo simulations, using the photometric performance of the new *Eddington* design, combined with more recent versions of the filtering and transit

detection algorithms, confirm these results (though over a much narrower range of parameter space). They also provide a testbed for the performance of the new algorithms, highlighting for example the presence of residual stellar micro-variability after filtering for more active stars. This shows that light curve filtering is an area where more progress could potentially be made. The results of similar Monte Carlo simulations for COROT confirmed the detectability of 'big hot Earths' with that mission. The case of COROT is explored in more detail in Chapter 6.